Surface Roughness by Contact versus Tapping Mode Atomic Force Microscopy

ARTICLE *in* LANGMUIR · JANUARY 1999

Impact Factor: 4.46 · DOI: 10.1021/la981024a

3 AUTHORS, INCLUDING:

Dana Sedin
New Belgium Brewing Company
5 PUBLICATIONS **197** CITATIONS

Surface Roughness by Contact versus Tapping Mode Atomic Force Microscopy

Garth J. Simpson, Dana L. Sedin, and Kathy L. Rowlen*

Department of Chemistry and Biochemistry, University of Colorado, Boulder, Colorado 80309

Received August 12, 1998. In Final Form: December 9, 1998

To evaluate and compare tapping mode and contact mode AFM measurements of surface roughness, images of quartz and mica were acquired by both methods and the height distributions and variance correlation functions analyzed. Significant deviation from the expected Gaussian profiles for the height distributions were observed for contact mode images of quartz but not for tapping mode images. Additionally, variance correlation functions were found to be highly scan size dependent for contact mode images and scan size invariant for tapping mode images. One possible explanation for the observed differences is that the scan speed limit is exceeded in contact mode for linear scan velocities as low as 0.5 μm/s.

Introduction

Surface roughness is of great importance for many technological applications requiring well-defined surfaces or interfaces.[1] Recently, scanning probe microscopies (SPMs) have been tested against standard surface roughness measurement techniques in order to evaluate their analytical utility for surface roughness determination.[2−5] While imaging artifacts in SPM,[6−10] such as those due to tip shape,[6] can influence roughness measurements, the general consensus appears to be that SPM can provide a reasonable measurement of surface roughness under appropriate conditions.

Of the two most common SPM techniques, scanning tunneling microscopy and atomic force microscopy (AFM), AFM has been more widely used for determination of surface roughness, since it can be applied to nonconducting surfaces. The two most common imaging modes for AFM are contact and intermittent contact, which is often referred to as tapping mode. There are two general approaches to contact mode imaging: constant height and constant force. Of these two, constant force is the most widely used. In constant force contact mode AFM,[11] the angle of a cantilever with respect to a probe beam is maintained at a preset value during lateral scanning by means of an electronic feedback loop, which adjusts the *z*-position of the piezoelectric scanner. In tapping mode AFM, the cantilever is oscillated near its resonant frequency. As the tip approaches the sample, the cantilever no longer oscillates freely but is affected by interaction with the surface.[12] Changes in either the amplitude, frequency, or phase of the oscillation may be used in a feedback loop. Typically, images are obtained from the voltage required to adjust the *z*-position of the piezoelectric scanner in order to maintain a preset amplitude of oscillation. Due to the nature of interaction between the sample and the tip in contact mode, the lateral forces are generally much greater than they are in tapping mode.[13]

Several researchers have employed tapping mode AFM to determine surface roughness,[2,3,7] while others have used contact mode.[4,5,8] Considering that the two imaging modes are fundamentally different with respect to how the tip interacts with the surface, the purpose of this study was to determine which imaging mode provides a more reliable measurement of surface roughness.

An important factor for comparing two surface roughness measurements is the mathematical approach employed in data analysis. While root-mean-square roughness (R_q) is perhaps the most universally reported measurement of surface roughness, due to the ease with which it may be determined and calculated, perhaps its greatest limitation is lack of spatial information.[7−10,12−14] R_q is calculated from height variations from a mean surface level (eq 1),

$$R_q = [\sum_{i=1}^{N}(z_i - z_m)^2/(N-1)]^{1/2} \quad (1)$$

in which N is the number of pixels in the image, z_i is the height of the ith pixel, and z_m is the mean image height. R_q values themselves are often difficult to interpret, since roughness is dependent on scan size, lateral and vertical resolution, and sampling density.[14] Additional insight can be gained by evaluating the distribution of surface heights. In the simplest case, the height distribution is Gaussian in nature (eq 2) and R_q is equal to the parameter σ,

$$P(z) = (1/\sigma\sqrt{2\pi})\exp[-(z - z_m)^2/2\sigma^2] \quad (2)$$

where $P(z)$ is the normalized probability of finding a particular height z. Non-Gaussian height distributions

* To whom correspondence should be addressed.

(1) Bhushan, B., Ed.; *Handbook of Micro/Nanotribology*; CRC Press: New York, 1995.
(2) Munkholm, A.; Brennan, S.; Carr, E. C. J. *Appl. Phys.* **1997**, *82*, 2944.
(3) Chu, P. K.; Brigham, R. G.; Baumann, S. M. *Mater. Chem. Phys.* **1995**, *41*, 61.
(4) Abe, T.; Steigmeier, E. F.; Hagleitner, W.; Pidduck, A. J. *Jpn. J. Appl. Phys.* **1992**, *31*, 721.
(5) Dumas, P.; Bouffakhreddine, B.; Amra, C.; Vatel, O.; Andre, E.; Galindo, R.; Salvan, F. *Europhys. Lett.* **1993**, *22*, 717.
(6) Westra, K. L.; Thomson, D. J. *J. Vac. Sci. Technol., B* **1995**, *13*, 344.
(7) Kiely, J. D.; Bonnell, D. A. *J. Vac. Sci. Technol., B* **1997**, *15*, 1483.
(8) Koinkar, V. N.; Bhushan, B. *J. Appl. Phys.* **1997**, *81*, 2472.
(9) Williams, J. M.; Beebe, T. P. *J. Phys. Chem.* **1993**, *97*, 6249.
(10) Williams, J. M.; Beebe, T. P. *J. Phys. Chem.* **1993**, *97*, 6255.
(11) The description of both imaging modes is based on the optical deflection design used in Digital Instrument's Nanoscope III.
(12) Burnham, N. A.; Behrend, O. P.; Oulevey, F.; Gremaud, G.; Gallo, P. J.; Gourdon, D.; Dupas, E.; Kulik, A. J.; Pollock, H. M.; Briggs, G. A. D. *Nanotechnology* **1997**, *8*, 67.
(13) Kasas, S.; Thomson, N. H.; Smith, B. L.; Hansma, P. K.; Miklossy, J.; Hansma, H. G. *Int. J. Imag. Sys. Technol.* **1997**, *8*, 151.
(14) Bennett, J. M.; Mattsson, L. *Introduction to Surface Roughness and Scattering*; Optical Society of America: Washington, DC, 1989.

10.1021/la981024a CCC: $18.00
Published on Web 01/22/1999

can provide additional information about the surface. For example, a height distribution skewed toward higher heights with respect to the mean is typical of a pitted surface.[14] Nevertheless, measurements of the height distribution function and R_q do not allow distinction between uniformly rough surfaces and generally smooth surfaces with relatively large-scale roughness features. Consequently, while height histograms can yield considerable insights in evaluating contact and tapping mode images, an additional, scale-dependent method of comparison is also desirable.

One alternative approach for evaluating surface roughness involves exploring the self-affine or fractal nature of surface features; in this case surface roughness is characterized by its dependence on scale.[15−18] While several mathematical methods are available for self-affine surface analysis (for example, power spectral methods,[19] contour and surface area analyses,[18,19] and multiple image variography[9,10]), correlation functions (or structure functions) have the advantages of simplicity and reliability.[18] A common height−height correlation function used to describe SPM images has been the Kohlrousch−Williams−Watts function (C_s):[20]

$$C_s(\tau) = \sigma_\infty^2 \exp -(\tau/\xi)^{2H}$$

$$\sigma_\infty \equiv \langle (z_\infty - z_m)^2 \rangle^{1/2} = R_q(\max)$$

$$\tau \equiv (x' - x, y' - y) \qquad (3)$$

where τ is the position vector in the $x-y$ surface plane, σ_∞ is the root-mean-square roughness at infinite separation (i.e., large with respect to ξ), ξ is the in-plane correlation length, z_∞ is the height at a lateral separation much greater than ξ, H is a scaling exponent, and the brackets indicate an expectation value. Together with H, the correlation length ξ determines the distance required in order to "lose memory" of an initial height and can be understood by the presence of relatively large surface features (e.g. "hills" and "valleys") giving rise to local structure that is gradually lost at larger distances. The exponent H is related to the local fractal dimension D by $D = 3 - H$.[15,19] For perfectly smooth, flat surfaces, $H = 1$ and $D = 2$, while, for an entirely fractal surface (i.e. self-similar at all size scales), $H = 0$ and $D = 3$. Random (Gaussian) noise exhibits $H = 0$.[21] Real surfaces are described by values of H between 0 and 1, as surfaces are assumed to be asymptotically flat at large size scales.

A more intuitive form for a correlation function utilizes the height−difference correlation rather than the height−height correlation:[15,17]

$$g(\tau) = \langle [z_0 - z_\tau]^2 \rangle = 2\sigma_\infty^2 [1 - \exp(-\tau/\xi)^{2H}] \qquad (4)$$

in which g is the mean squared height difference (i.e. the variance) as a function of lateral separation, z_0 is the height at an initial point on the surface, and z_τ is the height evaluated at a separation of τ. In the asymptotic case of large distances, the variance approaches twice the macroscopic (micrometer scale) variance $(R_q)^2$. At small distances with respect to ξ, the value of the variance correlation function is typically significantly smaller than the macroscopic variance. Note that σ_∞, H, and the in-plane correlation length ξ should be independent of scan size.

In this study, R_q values, height distributions, and variance correlation functions were employed as a means to compare contact and tapping mode AFM measurements of surface roughness. Mica was used as a smooth surface by which instrumental noise could be evaluated. Quartz was used as a representative rough surface. Roughness was evaluated as a function of surface type, scan size, and linear scan velocity.

Experimental Section

Tapping mode atomic force micrographs were obtained on a Digital Instruments Nanoscope IIIa. Contact mode images were obtained on a Digital Instruments Nanoscope E with the same scanner (2202E, 14.5 μm lateral range) used for tapping mode imaging. Etched single-crystal silicon tips with rectangular, single-beam cantilevers were used for both imaging modes: TESP for tapping and ESP for contact (Digital Instruments). ESP and TESP tips have essentially the same nominal tip radius (5−20 nm), but the cantilevers have quite different spring constants, 0.02−0.1 N/m for ESP and 20−100 N/m for TESP.[22] The resonance frequency is reported to be ∼5−20 kHz for ESP cantilevers and 200−400 kHz for TESP cantilevers. The quality factor (Q) for the two types of cantilevers was determined using the cantilever tune function with the tip far from a surface. Specifically, the resonance frequency (ω_0) and width ($\Delta\omega$) at $1/\sqrt{2}$ (∼70%) of the peak height (using amplitude as the vertical axis) were measured during cantilever oscillation in air. The quality factor was then calculated from $\omega_0/\Delta\omega$. Q was found to be ∼450−500 for TESP cantilevers and 30−40 for ESP cantilevers.

Tapping mode imaging conditions were as follows unless otherwise indicated: scan rate, 1.97 Hz; 512 points collected per line; z range equal to 1 nm for mica and 2 nm for quartz; integral gain at 0.6 and proportional gain at 0.6. The approximate amplitude of oscillation, calculated from the peak height in the cantilever tune mode, was 10 nm with a drive amplitude of ∼170 mV. The amplitude set point and engage set point were both ∼1 V. Constant force contact mode imaging conditions were exactly the same as those for tapping mode except that the integral gain was set at 1.0 and the proportional gain at 0.5. For contact mode the set point was ∼ −1 V. Typical pull-off forces were ≤1 nN for the 20−30% relative humidity conditions used in this study.

Mica surfaces were freshly cleaved just prior to analysis. Quartz (Esco, S1-UVB) was cleaned by sequential sonication (∼5 min) in 1.0 M potassium hydroxide, distilled water, hexanes, chloroform, and methanol. After cleaning, the quartz surface was dried under a flow of USP nitrogen. The typical relative humidity in the laboratory was 30−50%. Force curves were acquired prior to, during, and after imaging in order to evaluate the nature and magnitude of tip−water layer−surface interaction. Observation of electrostatic attraction to the surface, coupled with very large pull-off forces, required the use of a polonium source (Static Master, 1c200) for discharge of the surface. The quality of each tip prior to analysis was evaluated by imaging either polystyrene nanospheres (50 nm diameter, tapping mode)[23] or a vapor-deposited silver film (∼5 nm thickness) on mica (contact mode).[24]

Images were acquired with the atomic force microscope located on an oil-suspended marble base (the base in Digital Instrument's top-view optical microscope), and all software controllable filters were turned off. For roughness calculations, the raw images were first rescaled to ∼90% of their original size, to avoid edge effects, and then flattened (second order) prior to analysis using the modify/flatten subroutine in the Nanoscope software (4.23r2). R_q was calculated using the analyze/roughness subroutine in the Nanoscope software.

(15) Palasantzas, G. *Phys. Rev. B* **1993**, *48*, 14472.
(16) Mitchell, M. W.; Bonnell, D. A. *J. Mater. Res.* **1990**, *5*, 2244.
(17) Pynn, R. *Phys. Rev. B* **1992**, *45*, 602.
(18) Almqvist, N. *Surf. Sci.* **1996**, *355*, 221.
(19) Talibuddin, S.; Runt, J. P. *J. Appl. Phys.* **1994**, *76*, 5070.
(20) Williams, G.; Watts, D. C. *Trans. Faraday Soc.* **1970**, *66*, 80.
(21) Madelbrot, B. B. *The Fractal Geometry of Nature*; W. H. Freeman and Co.: San Francisco, 1983; p 250.
(22) *Nanoscope Command Reference Manual*, v. 4.22ce; Digital Instruments: 1997.
(23) Ramirez-Aguilar, K. A.; Rowlen, K. L. *Langmuir* **1998**, *14*, 2562.
(24) Roark, S. E.; Rowlen, K. L. *Chem. Phys. Lett.* **1993**, *212*, 50.

Prior to the calculation of variance correlation functions, AFM images were ASCII-exported to a double array, using the Nanoscope software, and numerically converted from integer format to decimal format with units of nanometers. To minimize noise due to scan drift along the slow scan axis, variance correlation functions were determined by calculating the variance $[z_{ij} - z_{(i+n)j}]^2$ along the lower-noise fast scan axis of the image double array as a function of the number of pixels n between the points (where z_{ij} is the height at a particular ij pixel location). The calculation was repeated for every accessible (at the edges some points are lost) pair of points in the 512 pixel by 512 pixel image, and the average result was saved in an array as a function of the separation distance in nanometers. The process was then repeated for values of n up to 50, and the data arrays were saved in a separate file.

Height histograms were calculated by first determining the highest and lowest points in the ASCII-exported integer image array and then selecting a histogram bin size to be 1/512 of the height difference between the minimum and maximum, yielding a final histogram with 512 bins. At each pixel location in the integer ASCII-exported image, the value of the integer describing the height at that point was compared with the value of the bin height as the bin height was incremented from the lowest point in the image. When the image height first exceeded the bin height, that bin was incremented by 1 and the analysis was repeated at the next pixel location until all points in the image were analyzed. The Nanoscope exported images have the image zero preset to the mean height of the image, allowing for exportation of histograms with a zero centered at the mean.

Results and Discussion

Since mica is atomically smooth over relatively large (often micrometer sized) areas, it served as reference point for comparison to "rough" surfaces. Obtaining atomic resolution with AFM requires meticulous attention to vibration isolation. In the absence of special precautions to isolate the instrument from vibrations, as was the case in this study, a smooth surface such as mica essentially provides a measure of instrumental noise. Figure 1 shows height histograms for mica imaged (1 μm) by contact mode (a) and tapping mode (b). As expected for random noise, the height histograms exhibited Gaussian distributions. A nonlinear regression fit of a Gaussian to the height distribution was used to extract a value for σ. For a statistically random surface, σ should be equal to R_q.

R_q values representative of surface roughness should scale with scan length (L) as $R_q \propto L^H$, where H is the scaling exponent.[7,9] Recall that $H = 0$ for random noise, such that the calculated R_q would be independent of L. Table 1 is a summary of R_q and σ values for both contact and tapping mode images of mica as a function of image scan size, from 125 nm to 5 μm. Note that, except for the largest scan sizes where contaminant features can be identified in the image, both R_q and σ are essentially independent of L. From five scan lengths, ranging from 125 nm to 2.5 μm, the mean R_q from tapping mode images of mica is 0.06 $\pm$ 0.02 nm. The mean R_q from the corresponding contact mode images of mica is 0.09 $\pm$ 0.02 nm. Within error, the instrumental noise for the two systems is the same.

Quartz. Figure 2 shows 2.5 μm $\times$ 2.5 μm top-view images of quartz obtained by tapping (a) and contact (b) mode AFM. The height distributions obtained from tapping mode images of quartz as a function of scan size are shown in Figure 3. Note that a Gaussian fit represents the distribution quite well from the smallest scan length of 125 nm up to ~2.5 μm. Table 2 summarizes the σ values extracted from the Gaussian fits. R_q values calculated directly from the images are also given in Table 2. For comparison, the height histograms obtained from contact mode images of the same piece of quartz as a function of scan size are given in Figure 4. The contact mode distributions show deviations from Gaussian behavior even at the smallest scan length. Both σ and R_q values are summarized in Table 2. Evaluation of Table 2 demonstrates a significant difference between the quartz surface roughnesses measured by tapping versus contact mode AFM. The measured R_q for tapping mode images of quartz can be as high as 63% different from R_q from contact mode images of the same 1 cm $\times$ 1 cm piece of quartz. For comparison, the typical relative error in measured R_q for both imaging modes is 2% (based on three or more measurements on the same surface).

As a first attempt to distinguish which of the two imaging modes yields a more representative measure of

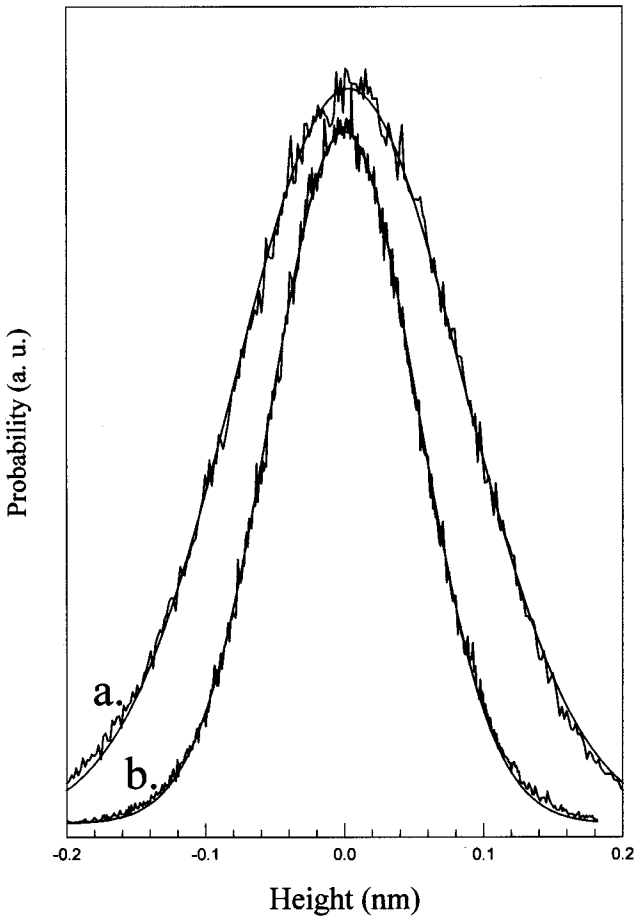

Figure 1. Height histograms for mica (1 μm $\times$ 1 μm) imaged by (a) contact and (b) tapping mode AFM. The smooth, solid lines are Gaussian fits (eq 2) to the respective histograms. The fitting parameter σ is summarized in Table 1 for various scan sizes. Truncation of the tapping mode histogram at high heights is a result of there being no points in the image with heights greater than those shown in the curve.

Table 1. Roughness Values from AFM Measurements on Mica

	tapping mode		contact mode	
scan size (nm)	R_q (nm)	σ (nm)	R_q (nm)	σ (nm)
125	0.052	0.050	0.075	0.080
250	0.053	0.052	0.13	0.080
500	0.054	0.052	0.082	0.081
1000	0.054	0.052	0.084	0.082
2500	0.087	0.058	0.090	0.079
5000	0.12	0.064	0.468	0.135

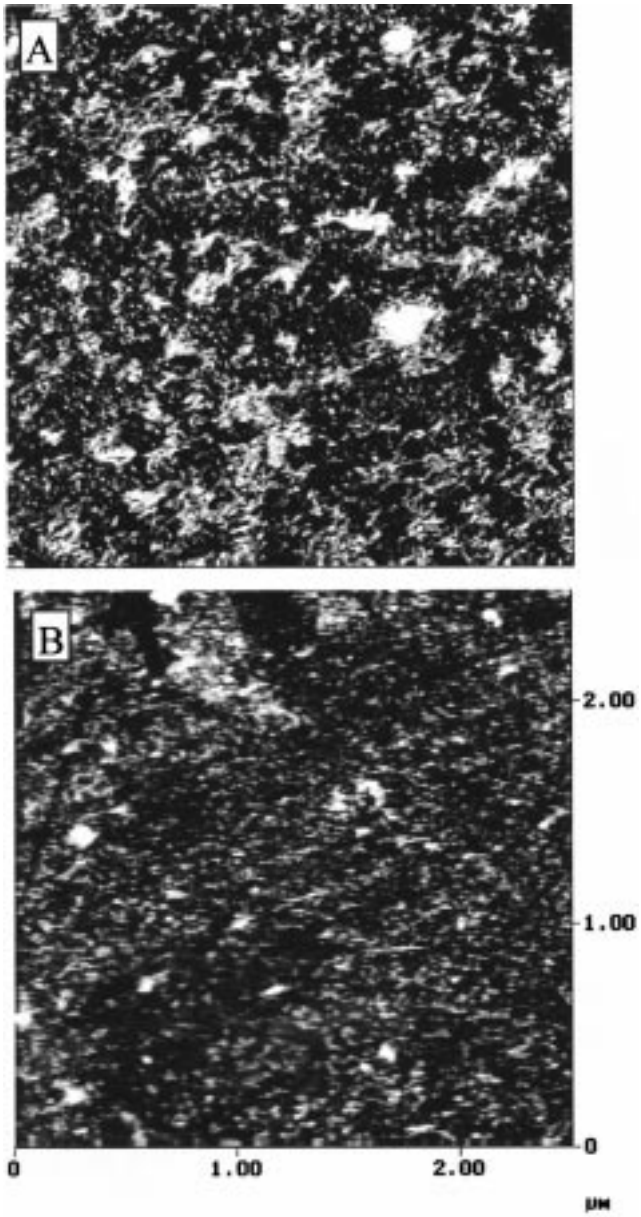

Figure 2. Tapping mode (A) and contact mode (B) images of the same piece of quartz (2.5 μm × 2.5 μm). The *z*-scale is 0 (dark) to 5 nm (light). Both images were obtained at a scan rate of 2 Hz with the contact force minimized prior to imaging.

surface roughness, σ was plotted versus R_q (Figure 5) and the correlation coefficients were determined for both tapping and contact mode. Tapping mode yields a squared correlation coefficient of 0.994, whereas the analogous correlation for contact mode is only 0.376. Clearly, the height distributions determined by contact mode do not represent the calculated surface R_q. It is important to point out that differences in tip shape cannot account for the observed differences in tapping and contact mode trends. Even though the two types of tips are expected to have very similar shape characteristics,[22] any discrepancies arising from differences in tip shape would be most significant at smaller scan sizes and diminish with increasing scan size.[25] In fact, the correlation between R_q and σ for contact mode gets progressively worse as the scan size increases, while good correlation between the two values is maintained for tapping mode over the entire scan range.

(25) Aué, J.; De Hosson, J. Th. M. *Appl. Phys. Lett.* **1997**, *71*, 1347.

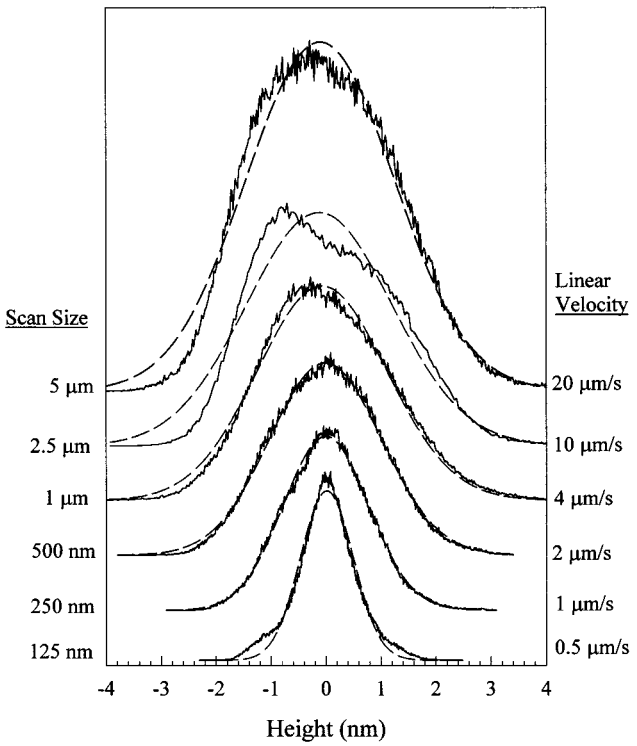

Figure 3. Height histograms for tapping mode images of quartz as a function of scan size. Gaussian fits are shown as dashed lines. The scan rate for all images was 2 Hz (2 lines/s). Corresponding linear scan velocities are reported to the right of the figure (the tip makes a round trip for each scan line; that is, a factor of 2 is required in the calculation of linear velocity).

Table 2. Roughness Values from AFM Measurements on Quartz[a]

	tapping mode		contact mode	
scan size (nm)	R_q (nm)	σ (nm)	R_q (nm)	σ (nm)
125	0.567	0.480	0.584	0.468
250	0.778	0.774	0.763	0.654
500	0.977	1.02	0.598	0.570
1000	1.17	1.18	0.798	0.665
2500	1.25	1.33	0.873	0.702
5000	1.32	1.34		

[a] Roughness parameters for the 5 μm contact mode image are not reported due to poor image quality.

The height variance correlation function given in eq 4 can be used to further investigate the reliability of roughness measurements. Plots of height variance as a function of lateral separation in one dimension should yield scan-size-invariant values for H, σ_∞, and ξ. Figure 6 is such a plot for both tapping (a) and contact (b) mode images of quartz. For tapping mode, all of the curves behave as expected, with the same rate of increasing variance with increasing lateral separation up to an asymptotic value. However, significant deviation is observed for contact mode, in both the degree of overlap and the location of the *knee* regime. The knee region is related to ξ and should be independent of scan size. Poor overlap in the variance correlation functions derived from contact mode images of rough surfaces has been previously reported.[18,26] Of interest with respect to this study is the contrast between tapping and contact mode. Qualitatively, the results for tapping mode are clearly superior to those for contact mode.

(26) Oden, P. I.; Majumdar, A.; Bhushan, B.; Padmanabhan, A.; Graham, J. J. *J. Tribol.* **1992**, *114*, 666.

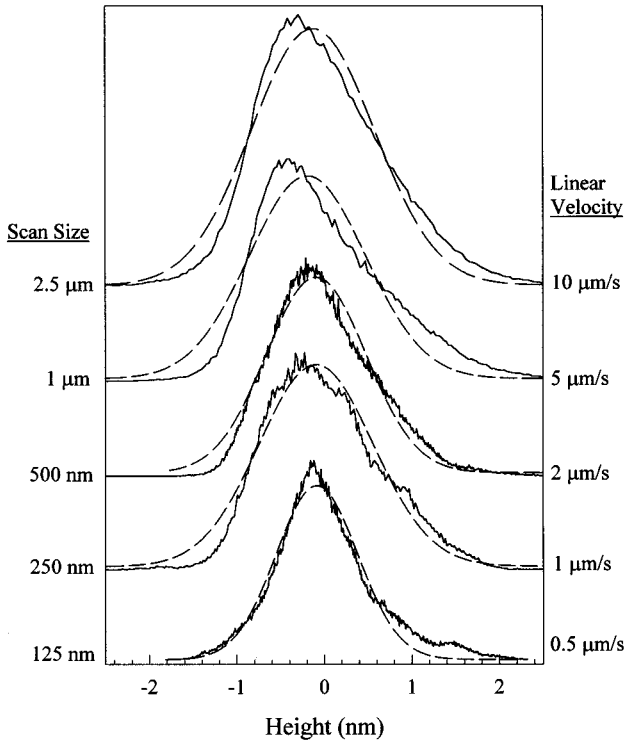

Figure 4. Height histograms for contact mode images of quartz as a function of scan size. Gaussian fits are shown as dashed lines. The scan rate for all images was 2 Hz (2 lines/s). Corresponding linear scan velocities are reported to the right of the figure.

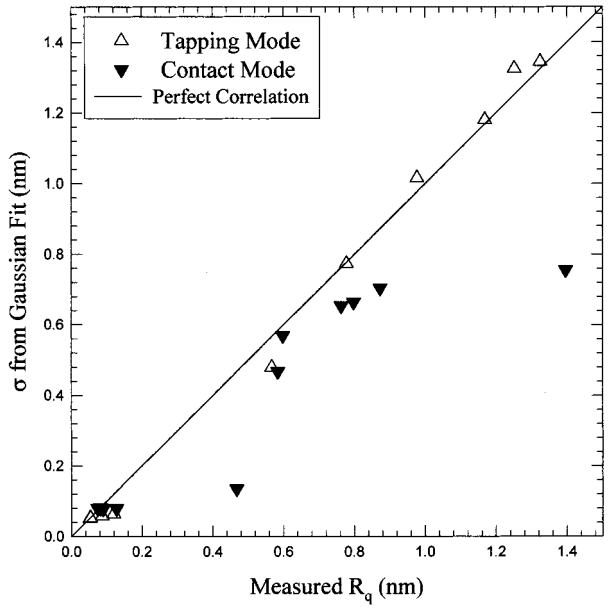

Figure 5. Correlation diagram for measured image R_q and σ values obtained from Gaussian fits to height histograms. The solid line represents a correlation of 1 (i.e., $x = y$). The correlation coefficient (r^2) is 0.994 for tapping mode and 0.376 for contact mode.

To provide a more quantitative comparison of the relevant parameters from analysis of height variance functions, values for H, ξ, and σ_∞ are summarized in Table 3. In calculating the variance correlation function parameters, the scaling exponent H was first determined from the slope of a log−log plot of the variance correlation function versus distance (in the limit of distances much less than ξ, $g(x) \propto x^{2H}$);[15] then ξ and σ_∞ were fit in a least-squares fashion to $g(x)$, as in eq 4. The most notable feature

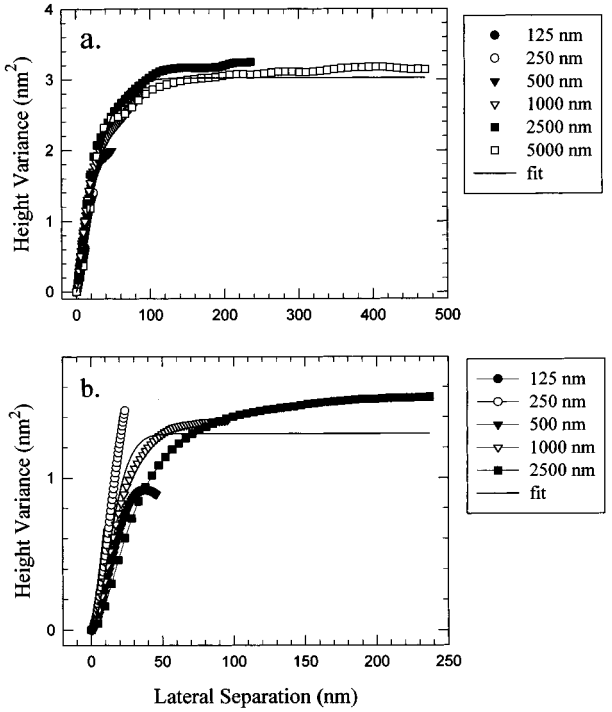

Figure 6. Variance correlation functions for quartz imaged by (a) tapping mode and (b) contact mode AFM. The data were evaluated along the fast-scan axis (i.e., $\tau = x$ in eq 4 and x = fast-scan axis). The trends are quite similar when evaluated with x = slow-scan axis. The solid lines are fits to eq 4: $H = 0.655$, $\sigma = 1.74$ nm, $\xi = 31.6$ nm, and $r^2 = 0.977$ for (a) and $H = 0.868$, $\sigma = 1.14$ nm, $\xi = 18.0$ nm, and $r^2 = 0.871$ for (b). Note the difference in vertical scale; tapping mode yields an asymptotic variance roughly twice that obtained by contact mode.

Table 3. Parameters Extracted from Analysis of the Variance Correlation Function[a]

	scan size (nm)	H	ξ (nm)	σ_∞ (nm)	R_q (nm)
tapping mode	125	0.73			0.567
	250	0.71			0.778
	500	0.63	16	1.00	0.977
	1000	0.65	23	1.14	1.17
	2500	0.52	30	1.26	1.25
	5000	0.68	35	1.24	1.324
	mean	0.66 ± 0.07	26 ± 8	1.16 ± 0.06	
contact mode	125 nm	0.82			0.584
	250 nm	0.87			0.763
	500 nm	0.90	18	0.68	0.598
	1000 nm	0.87	22	0.82	0.798
	2500 nm	0.82	40	0.86	0.873
	mean	0.86 ± 0.04	27 ± 12	0.79 ± 0.03	

[a] These values were obtained from fits to eq 4, in which the fast-scan axis data were used as the x variable. Values obtained from the same analysis using the slow-scan axis (available upon request) were quite comparable. Only the first 50 points of the correlation functions were used to fit the data, as the functions exhibit significant deviations at larger separations.[16] Values are not reported for 125 and 250 nm scan sizes, since the first 50 points do not extend the function past the knee region.

of the tabulated results is the greater scan size dependence of the correlation length ξ in contact mode than in tapping mode. The relative error in ξ is reasonably poor for both imaging modes but is worse for contact (46%) than for tapping mode (32%). The relative error in H is comparable for both contact and tapping mode (4% and 5%, respectively). Extracted σ_∞ values agree quite well with calculated R_q values for both imaging modes, although the mean

σ_∞ for tapping mode is 47% greater than the mean σ_∞ for contact mode.

All of the experimental results taken together suggest that tapping mode provides a more accurate measure of surface roughness than does contact mode. However, there is evidence that capillary and adhesion forces can influence tapping mode height measurements. For example, Van Noort and co-workers reported height artifacts in tapping mode images that resulted in an underestimation of feature height of up to 10 nm.[27] In the data presented here, the opposite appears to be true. For example, the variance correlation functions shown in Figure 6 provide evidence that contact mode imaging underestimates the height variation. The asymptotic value for height variance in tapping mode is approximately twice that obtained by contact mode. This effect may be associated with lateral friction forces in contact mode that are negligible in tapping mode—high frictional forces leading to poorer height resolution in contact mode. As an independent test of the reliability of tapping mode height measurements in a humid environment (relative humidity being the largest contributor to adhesion forces for these systems), we compared AFM and transmission electron microscopy (TEM) images of individual polystyrene nanospheres.[28] The heights of five separate nanospheres, as measured by tapping mode AFM, differed by less than 5%, on average, from the widths measured by TEM. Thus, the tapping mode data are deemed reliable.

One possible explanation for the observed trends is the scan speed limit.[29] In both imaging modes, the scan speed limit is determined by the instrument response time to a change (in cantilever deflection for contact mode or cantilever amplitude of oscillation for tapping mode). When the linear velocity used for scanning exceeds an upper limit, the system cannot respond fast enough to small changes in cantilever position (or oscillation amplitude); thus, surface features may be "missed." The scan speed limit is probably established by the cantilever response time, which is often expressed in terms of a time constant (τ):

$$\tau = \frac{2Q}{\omega_0} \tag{5}$$

where Q is the quality factor and ω_0 is the resonance frequency. Using measured values for Q and ω_0 (see Experimental Section), a τ of $\sim$3 ms is calculated for TESP cantilevers and one of $\sim$10 ms is calculated for ESP cantilevers. Thus, because of their design, tapping mode tips have approximately a three time faster response time than contact mode tips.

Experimental evidence for scan speed limitations may be found in the height distribution functions (Figures 3 and 4). While all of the images used in this study were acquired at a scan rate of 2 Hz, the linear velocity, or scan speed, depends on the scan size. As noted in the figures, the linear velocity ranges from 0.5 to 20 μm/s. Deviations from a Gaussian distribution as a function of scan size are likely due to features on the surface that are not quantified. As can be observed in Figure 3, for tapping mode the deviations from Gaussian do not become significant until the linear velocity exceeds 4 μm/s. For contact mode (see Figure 4), significant deviations are observed at linear velocities as low as 1 μm/s.

As a crude estimate, the scan speed limit may be calculated by dividing a given scan size by the minimal time required to adequately sample every point in a linear scan. That minimal time can be calculated from the product of the cantilever time constant (τ) and the number of points sampled per line. Using a 1 μm scan size, 512 points per line, and τ = 3 ms, the scan speed limit is estimated to be $\sim$0.7 μm/s for tapping mode imaging in air. Using the same parameters and τ = 10 ms, the scan speed limit is estimated to be $\sim$0.2 μm/s for contact mode imaging in air. While these rough calculations yield limits less than the points at which significant deviations in the height distribution functions are observed, the relative limits are in surprisingly good agreement with observations (the scan speed limit for contact mode being approximately three to four times less than that of tapping mode).

Acknowledgment. The authors gratefully acknowledge funding from the National Science Foundation.

LA981024A

(27) Van Noort, S. J.; Van der Werf, K. O.; DeGrooth, B. D.; Van Hulst, N. F.; Greve, J. *Ultramicroscopy* **1997**, *69*, 117.
(28) Ramirez-Aguilar, K. A.; Rowlen, K. L. *Langmuir* **1998**, *14*, 2562.
(29) Butt, H. J.; Siedle, P.; Seifert, K.; Fendler, K.; Seeger, T.; Bamberg, E.; Weisenhorn, A. L.; Goldie, K.; Engel, A. *J. Microsc.* **1993**, *169*, 75.